RSC Advances

PAPER

Cite this: *RSC Adv.*, 2020, **10**, 1232

Antibacterial potential of Ni-doped zinc oxide nanostructure: comparatively more effective against Gram-negative bacteria including multi-drug resistant strains

Atanu Naskar, † Sohee Lee † and Kwang-sun Kim *

Infections by multidrug-resistant (MDR) bacteria are one of the most threatening concerns for public health. For this purpose, nanomaterials have emerged with great potential for antibacterial activity. In this paper, we report the synthesis of new Ni^{2+}-doped zinc oxide (Ni-ZnO or NZO) nanostructures as targeted antibacterial agents for Gram-negative bacteria. A one-pot low-temperature solution process was used with varying compositions containing 2 or 5% Ni^{2+} relative to Zn^{2+}, resulting in 2NZO or 5NZO, respectively. X-ray diffractometry, transmission electron microscopy, and X-ray photoelectron spectroscopy were used for material characterization. Further, the antibacterial activity against both Gram-negative [*Escherichia coli* (*E. coli*) and *Acinetobacter baumannii* (*A. baumannii*) strains including standard, MDR, and clinical isolates associated with *mcr-1* gene] and Gram-positive (*Staphylococcus aureus* and *Staphylococcus epidermidis*) bacteria were evaluated through analysis of zone of inhibition, minimum inhibitory concentration (MIC), and scanning electron microscopy images. Among the prepared nanostructures, the 5NZO sample showed excellent antibacterial activity against MDR strains of *A. baumannii* and *E. coli*. In addition, samples of NZO generated approximately 7 to 16 times more reactive oxygen species (ROS) in *E. coli* compared to ZnO. Our synthesized nanomaterials have the potential to fight MDR and colistin-resistant Gram-negative bacteria.

Received 14th November 2019
Accepted 26th December 2019

DOI: 10.1039/c9ra09512h

rsc.li/rsc-advances

1. Introduction

One of the most urgent challenges threatening global public health care systems is infection related to multidrug-resistant (MDR) microorganisms.[1] Multidrug resistance is defined as the resistance of microorganisms, and their increasing resistance, against at least two currently administered antimicrobial medications that used to be effective.[2] This has a profound impact on public health, as predictions indicate that there will be 10 million annual deaths due to MDR pathogens by 2050, which is higher than that of cancer, unless immediate interventions are developed.[3] The grim reality is that human beings will face a time when no antibiotic will act against even a simple bacterial infection if proper action is not taken immediately. At present, some bacterial strains, such as methicillin-resistant *Staphylococcus aureus* (MRSA) cannot be treated with the last resort antibiotic vancomycin, as a result of the evolution of vancomycin-resistant *Staphylococcus aureus* (VRSA) strains.[4] In addition, the rate of antibiotic development is far less than the attainment of resistance by MDR bacteria.[5] Therefore, it is clear that alternatives to traditional antibiotics, such as antibacterial materials, need to be swiftly developed or discovered to fight against MDR bacterial cells.

Among many different MDR bacterial cells that require immediate intervention, Gram-negative *Acinetobacter baumannii* (*A. baumannii*) is one of 12 families of priority pathogenic bacteria identified by the World Health Organization (WHO) as a major threat to the clinical treatment of infections in human beings.[6] This pathogen is mainly found in hospital settings, where critically ill hospitalized patients are exposed through cracks in the skin and respiratory tract.[7] In addition, Gram-negative *Escherichia coli* (*E. coli*) is the main culprit behind urinary tract infections (UTIs)[8] and water borne diseases.[9] An epidemiological survey on cystitis, the inflammation of the bladder usually caused by UTIs, showed that more than 10% of *E. coli* isolates are MDR.[10] According to the WHO, unsafe water is reported as the main reason behind 80% of all diseases,[11] with *E. coli* being a member of the fecal coliforms that frequently contaminate drinking water.[9] Therefore, alternative antibacterial materials are immediately needed to counter MDR strains of both *E. coli* and *A. baumannii* strains.

Alternative approaches to conventional antibiotics to fight bacterial infections include combinations of antibiotics,[1]

Department of Chemistry and Chemistry Institute for Functional Materials, Pusan National University, Busan 46241, South Korea. E-mail: kwangsun.kim@pusan.ac.kr; Tel: +82-51-510-2241

† Both authors contributed equally to this paper.

antibacterial antibodies,[12] bacteriophages,[13] photothermal therapy,[14] and nanomaterials.[15] Among these alternatives, nanomaterials composed of Ag,[16] Au,[17] ZnO,[18] CuO,[19] TiO_2,[20] graphene,[21] and black phosphorus[22] are increasingly attracting attention for antibacterial development due to their favorable physiochemical properties. Zinc oxide (ZnO) is one of the most promising nanomaterials as an antibacterial agent due to its effective antibacterial activity and selectivity for bacterial cells, while being minimally toxic to human cells; it is one of the five zinc compounds approved by the U.S. Food and Drug Administration (21CFR182.8991) as a safe antibacterial agent.[18] Due to its biocompatible properties, ZnO has already been used as an antibacterial agent in the preparation of various commercial products such as medical equipment, food packaging materials, and cosmetics.[23]

Moreover, there are several reports describing the particle size-dependent antibacterial activity of ZnO nanoparticles (NPs), where antibacterial activity is inversely correlated with particle size.[24] Hence, the particle size of ZnO NPs needs to be reduced to achieve better antibacterial activity. In this regard, doping ZnO with trace amounts of metal ions has shown significant changes in the physical and chemical properties of ZnO NPs, including particle size.[25] Several reports are available regarding the doping of ZnO with metal ions of Ni, Co, Fe, Mn, Cr, Al, and Ag to change its properties for photocatalysis, sensors, and antibacterial activity.[26–32] Among the above dopants, Ni^{2+} is favorable to incorporate into the ZnO lattice due to its same valence state (+2) and similar ionic radii (Ni^{2+}, 0.69 Å; Zn^{2+}, 0.74 Å). Moreover, various reports regarding the antibacterial activity of metal ion-doped ZnO, Ag,[27,28] Co,[29,30] and Cr[31,32] have been reported. For instance, the work reported by Dias *et al.*[27] has shown the antibacterial activity of Ag doped ZnO nanoparticles against *S. mutans*. Similar work was also shown with *E. coli* by Karunakaran *et al.*[28] Moreover, the work by Vijayalakshmi *et al.*[31] has shown the antibacterial activity of Cr doped ZnO nanorods against *E. coli* and *S. aureus*. Meanwhile, the use of Ni^{2+} as a dopant for ZnO with regard to antibacterial activity against MDR bacteria is sorely lacking.

Despite the excellent antibacterial property possessed by Ni^{2+}-doped ZnO (NZO) NPs/nanostructures, very few reports are available regarding its against MDR pathogens. Therefore, the objective of the present work is to synthesize an effective nanomaterial of NZO NPs and nanostructures as a potential alternative to traditional antibiotics for the fight against MDR bacteria. Herein, we report a one-pot synthesis of NZO NPs prepared using a low-temperature solution process and their antibacterial activity compared to ZO NPs/nanostructures against the Gram-negative bacteria, *E. coli* and *A. baumannii* including their MDR strains [*E. coli* 1368, BAA2452, and 1A626 and *A. baumannii* (12001)] and colistin-resistant clinical isolates harboring *mcr-1* gene.

2. Material and methods

2.1 Synthesis of Ni^{2+}-doped ZnO (NZO) nanostructures

Briefly, 0.1 M of zinc nitrate hexahydrate [$Zn(NO_3)_2 \cdot 6H_2O$, Merck] and nickel sulfate hexahydrate ($NiSO_4 \cdot 6H_2O$, Sigma-Aldrich, 99%) are used to prepare 0, 2, and 5 atomic percent (at%) (with respect to Zn^{2+}) ZnO-based NPs. The mixtures were uniformly dispersed in a beaker containing 50 mL of deionized water with continuous stirring for 30 min at room temperature. While continuing to stir, 1 mL of hydrazine hydrate ($N_2H_4 \cdot H_2O$, Merck, 99–100%) was added dropwise to the reaction mixture. After complete addition, the mixture was ultrasonicated for 10 min at 60 °C in a water bath ultrasonicator until a slightly pink precipitate was observed at the bottom of the reaction flask. Further dropwise addition of hydrazine hydrate and ultrasonication was repeated until the pH of the medium reached 8. Afterward, the precipitate was separated by centrifugation. Deionized water and ethanol were then used to wash the product 3–4 times. Finally, the product was dried in an oven at ~60 °C for 24 h. The synthesized ZnO-based NPs containing 0, 2, and 5 at% Ni are referred to as ZO, 2NZO, and 5NZO, respectively.

2.2 Characterizations

2.2.1 Material properties. X-ray diffractometry (XRD) using an X-ray diffractometer (D8 Advance with DAVINCI design X-ray diffraction unit, Bruker) with nickel filtered Cu K_α radiation source ($\lambda = 1.5406$ Å) was used in the 2θ range 20–80° to collect the diffraction patterns and assess the structures of ZO, 2NZO, and 5NZO. Moreover, transmission electron microscopy (TEM; Bruker Nano GmbH) using carbon coated 300 mesh Cu grids for placement of the samples was employed for microstructural analysis. An Axis Supra Scanning X-ray photoelectron spectroscopy (XPS) microprobe surface analysis system was used to assess a representative sample of 5NZO by scanning a binding energy range of 200–1200 eV to determine the chemical state of elements. The C 1s peak position at 284.5 eV was used as the binding energy reference.

2.2.2 Growth of bacteria for evaluation of antibacterial activity. Bacterial strains of *E. coli* (ATCC 25922), *A. baumannii* (ATCC 19606), *S. aureus* (ATCC 25923), *Staphylococcus epidermidis* (*S. epidermidis*, ATCC 12228), and MDR strains of *E. coli* (1368, BAA2452, and 1A626) and *A. baumannii* (12001) were grown in a BBL™ Mueller–Hinton Broth (MHB, Becton Dickinson) culture medium. Single colonies of bacteria were inoculated into MHB and incubated at 37 °C overnight, followed by dilution of the cells to an optical density of 0.5 McFarland turbidity standard using a Sensititre™ Nephelometer (Thermo Scientific). After dilution, the cell cultures were used within 30 min to prepare samples for the agar well diffusion method to assess both antibacterial activity of NPs (ZO, 2NZO, and 5NZO) and morphological characterization (Sections 2.2.3 and 2.2.4).

2.2.3 Agar well diffusion method for evaluation of antibacterial activity. The agar well diffusion method was used to evaluate the antibacterial activity of ZO, 2NZO, and 5NZO against the bacterial strains prepared in Section 2.2.2 (*i.e.*, *E. coli*, *A. baumannii*, *S. aureus*, *S. epidermidis*, and MDR strains of *E. coli* and *A. baumannii*). In brief, 500 μL of cultured bacterial cells was mixed with 25 mL of MHB-agar, poured into sterile Petri dishes (SPL), and solidified. Then, using a sterile plastic rod, five holes (6 mm in diameter) were aseptically punched

through the surface. Thereafter, 20 μL (5 mg mL^{-1}) of ZnO-containing samples as (i) ZO, (ii) 2NZO, and (iii) 5NZO were added; followed by a positive control (iv) of 20 μL (5 mg mL^{-1}) of either polymyxin B or ampicillin (Sigma-Aldrich), for Gram-negative or -positive strain, respectively; and a negative control (v) of 20 μL of dimethyl sulfoxide (DMSO; Sigma-Aldrich). The plates were then incubated for 24 h at 37 °C and the antibacterial activities were evaluated by measuring the diameter of the zone of inhibition (ZOI) around the wells using a ruler.

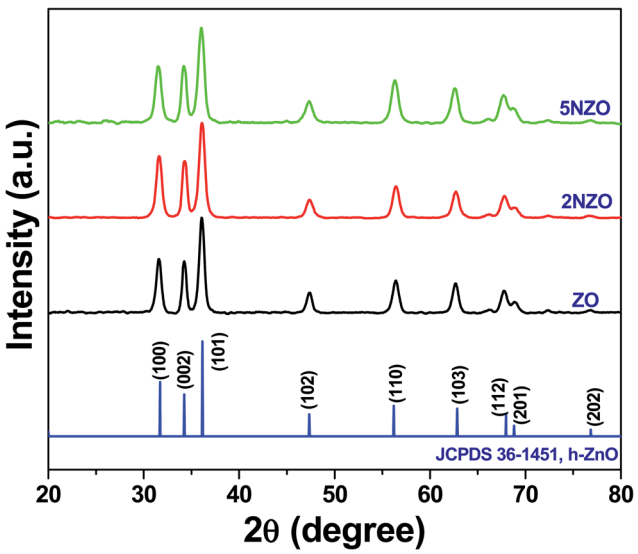

Fig. 1 XRD patterns of ZO, 2NZO, and 5NZO samples.

2.2.4 Minimum inhibitory concentration (MIC) for evaluation of antibacterial activity. MIC was determined by micro-broth dilution method as described. Briefly, bacterial cells (0.5 McFarland turbidity) were mixed with nanomaterials (ZO, 2NZO, and 5NZO) varying from 10 to 250 μg mL^{-1} range in a 96-well microplate. The resulting mixtures were incubated at 37 °C for 16 h with 500 rpm shaking using Incu-Mixer™ MP (Benchmark Scientific). The nanomaterial concentration that completely inhibit the bacterial growth was defined as MIC value.

2.2.5 Morphological characterization of bacteria. Initially, 500 μL of bacterial cells in Section 2.2.2 with 20 μL (5 mg mL^{-1}) of 5NZO were incubated for 4 h at 37 °C with vigorous shaking. A pellet from the cell cultures was harvested by centrifugation at 12,000 rpm for 5 min and this pellet was resuspended in 500 μL of phosphate buffered solution (pH 7) containing 2% formaldehyde and 1% glutaraldehyde, and then centrifuged again. The obtained cell pellet was washed twice with deionized water and then resuspended in 1 mL of deionized water. From this suspension, a 5 μL aliquot was deposited on a silicon wafer

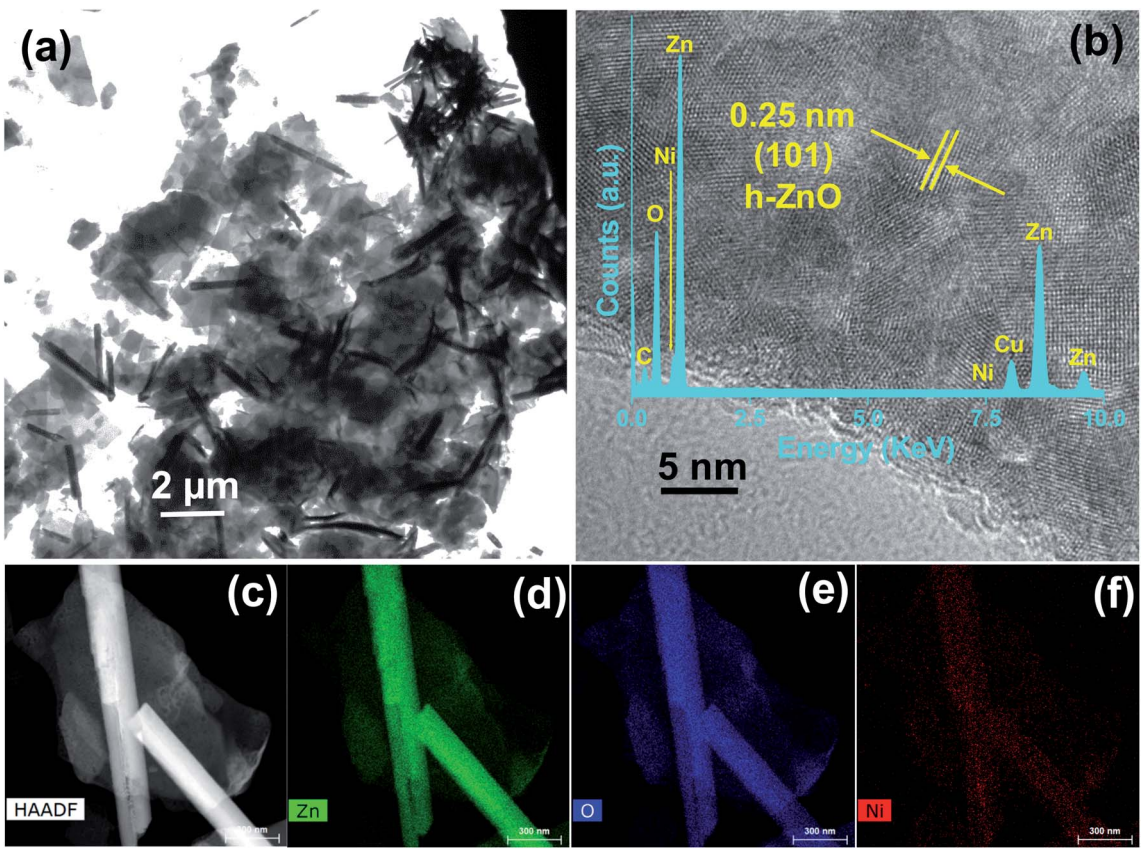

Fig. 2 5NZO sample (a) TEM image, (b) HRTEM image with (b inset) TEM-EDS spectrum, (c) HAADF image, and element mappings of (d) Zn, (e) O, and (f) Ni.

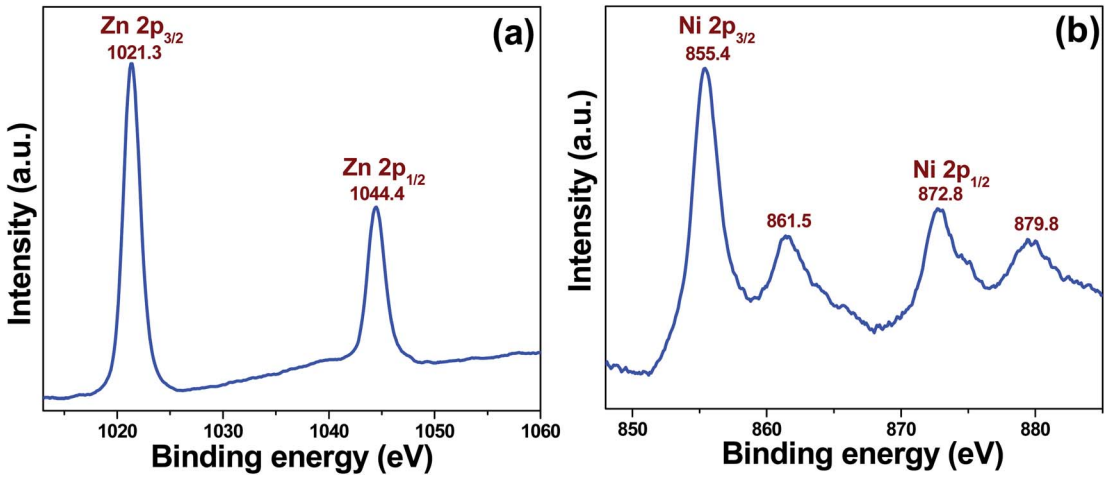

Fig. 3 XPS binding energy spectra of 5NZO (a) Zn 2p and (b) Ni 2p core levels.

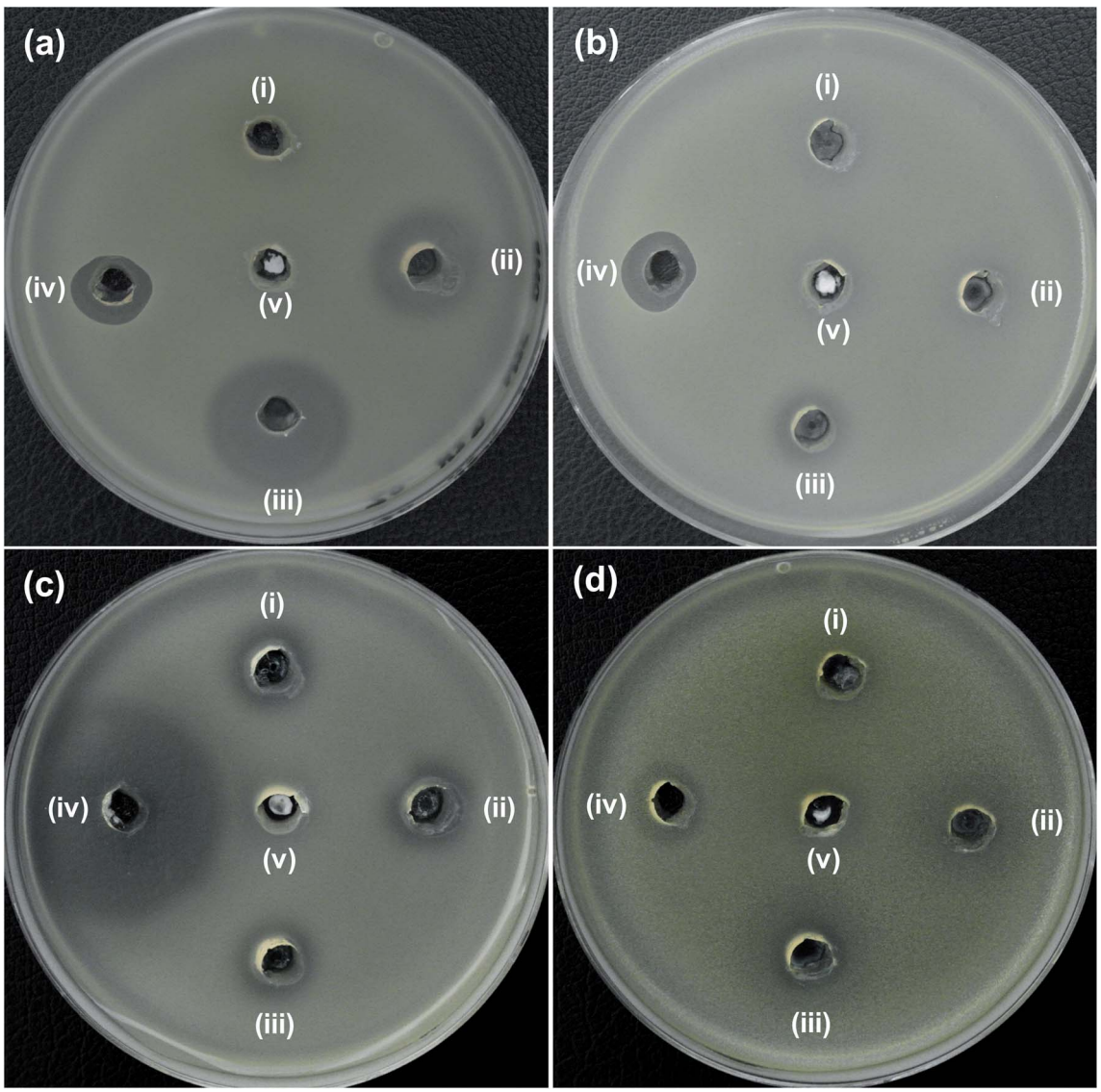

Fig. 4 Zone of inhibition (ZOI) of ZnO samples against (a) *E. coli*, (b) *A. baumannii*, (c) *S. aureus* and (d) *S. epidermidis*. Diameter of ZOI is also displayed in the Table 1 (average from $n = 3$).

(5 mm × 5 mm in size, Namkang Hi-Tech Co., Ltd) and air-dried to subject scanning electron microscopy (SEM) analysis using VEGA3 (TESCAN), a versatile tungsten thermionic emission SEM system according to the manufacturer's protocol.

2.2.6 Determination of reactive oxygen species (ROS) production. The production of ROS by *E. coli* ATCC 25922 after treatment with ZnO nanorods was evaluated based on the previous reports.[33] Briefly, the adjusted bacterial culture (0.5 McFarland turbidity) in PBS buffer by Sensititre™ Nephelometer (Thermo Scientific) was treated with different concentrations of nanomaterials corresponding to 0, 125, 200, and 250 μg mL^{-1} in the presence of 2′,7′-dichlorodihydrofluorescin diacetate (DCFH-DA) (Sigma-Aldrich) at a final concentration of 30 μM in PBS buffer. The mixtures in 96-well plate were incubated at 37 °C with vigorous shaking (500 rpm) using Incu-Mixer™ MP (Benchmark Scientific) for 45 min. Then, the fluorescence intensity was measured by a FLUOstar Omega (BMG Labtech) with an excitation and emission wavelengths of 485 and 520 nm, respectively. Untreated bacterial culture was used as a negative control and the background fluorescence of PBS and autofluorescence of the bacterial cells incubated without the probe was measured to calculate the net fluorescence emitted from the assay itself. The data was further analyzed using MARS Data Analysis software (ver. 3.02 R2, BMG Labtech) and the relative ROS production of samples treated with increasing concentrations of NPs was compared to non-NP treated samples from triplicate experiments with $p < 0.05$.

3. Results and discussion

3.1 Material properties

3.1.1 Phase structure. X-ray diffraction patterns of synthesized ZO, 2NZO, and 5NZO were obtained, consistent with hexagonal ZnO (h-ZnO) [JCPDS 36-1451] (Fig. 1). As only the ZnO peaks are observed, samples were regarded as pure, containing the ZnO lattice substituted with Ni^{2+} ions. Moreover, a slight shift in 2θ values towards higher diffraction angles was observed for both of the Ni^{2+}-doped samples (2NZO and 5NZO) compared with ZO, suggesting successful incorporation of Ni^{2+} in the ZnO crystal lattice.[26]

The average crystallite size (D) of ZnO crystallites was measured along the (101) crystal plane using the Debye–Scherrer eqn (1).

$$D = k\lambda/\beta \cos\theta, \quad (1)$$

where k is the proportionality constant ($k = 0.89$), λ is the X-ray wavelength (1.5406 Å), β is the full width at half maximum of the peak of maximum intensity in radians, θ is the diffraction angle, and D is the crystallite size.

The measured D values of ZO, 2NZO, and 5NZO after solving eqn (1) were approximately 27, 25, and 21 nm, respectively. Therefore, ZnO crystallite size decreases with increasing Ni^{2+}-doping concentration in the precursor solutions. The gradual decrease in D with increasing Ni^{2+} concentration can be attributed to substitution with Ni^{2+} ions in the ZnO crystal

Table 1 Zone of inhibition (ZOI) diameter of ZnO samples against (a) *E. coli* and (b) *A. baumannii*, (c) *S. aureus*, and (d) *S. epidermidis* was measured from $n = 3$ and one of the representative data was shown. N.D. indicates that the zone of inhibition was not detected[a]

	Zone of inhibition (mm)				
Bacteria cells	(i) ZO	(ii) 2NZO	(iii) 5NZO	(iv) Antibiotics	(v) DMSO
(a) *E. coli* ATCC25922	N.D.	18	24	14[a]	N.D.
(b) *A. baumannii* ATCC19606	N.D.	N.D.	12	13[a]	N.D.
(c) *S. aureus* ATCC25923	13	14	14	38[b]	N.D.
(d) *S. epidermidis* ATCC12228	N.D.	11	14	14[b]	N.D.

[a] Antibiotics, [a]Polymyxin B or [b]Ampicillin was used as a control for Gram-negative or -positive bacteria, respectively.

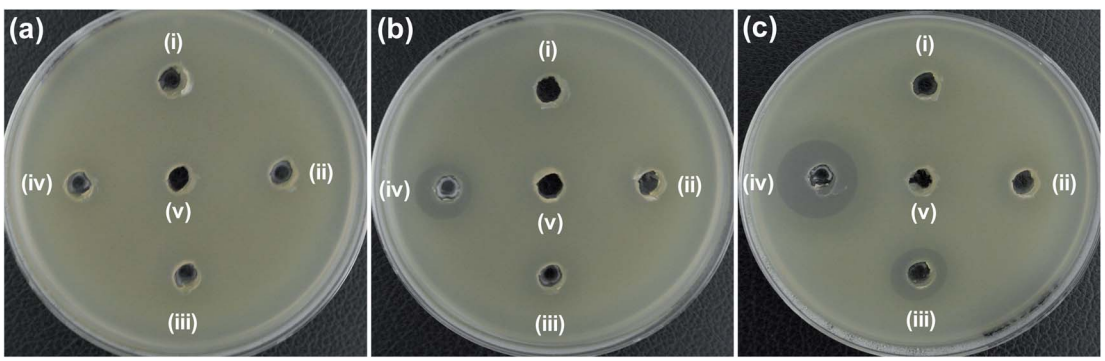

Fig. 5 Zone of inhibition (ZOI) of (a) ZO, (b) 2NZO and (c) 5NZO samples against *E. coli* at different concentrations. Diameter of ZOI is also displayed in the Table 2 (average from $n = 3$).

Table 2 Zone of inhibition (ZOI) diameter of (a) ZnO, (b) 2NZO, and (c) 5NZO samples against *E. coli* at different concentrations. N.D. indicates that the zone of inhibition was not detected[a]

	Zone of inhibition (mm)			
Samples	(i) 0.5 mg mL^{-1}	(ii) 1.25 mg mL^{-1}	(iii) 2.5 mg mL^{-1}	(iv) 5 mg mL^{-1}
(a) ZnO	N.D.	N.D.	N.D.	N.D.
(b) 2NZO	N.D.	N.D.	N.D.	15
(c) 5NZO	N.D.	N.D.	15	20

[a] DMSO (v) was used as negative control in all Petri dishes.

lattice.[26] It appears that the surface area increases due to decreasing ZnO crystallite size, potentially resulting in better antibacterial activity.

3.1.2 Morphology and microstructure. TEM was utilized to further investigate the shape and size of ZnO NPs. The TEM image of 5NZO (Fig. 2a) shows the formation of ZnO nanorods ranging from 2.0 to 3.0 μm in length with diameters from 150 to 200 nm. The presence of hexagonal ZnO is confirmed by high-resolution TEM (HRTEM; Fig. 2b), whereby distinct lattice fringes with an interplanar distance of 0.25 nm correspond to the (101) plane of hexagonal ZnO.[34] Therefore, TEM and HRTEM support the XRD results (Fig. 1). Furthermore, TEM with energy-dispersive X-ray (TEM-EDX) spectral analysis of the 5NZO was performed and is shown in the inset of Fig. 2b. The presence of Zn and O in the TEM-EDX spectrum also support the formation of ZnO NPs; moreover, identification of Ni suggests the incorporation of Ni^{2+} ions in the ZnO lattice. C and Cu in the TEM-EDX spectrum arises from the carbon coated Cu

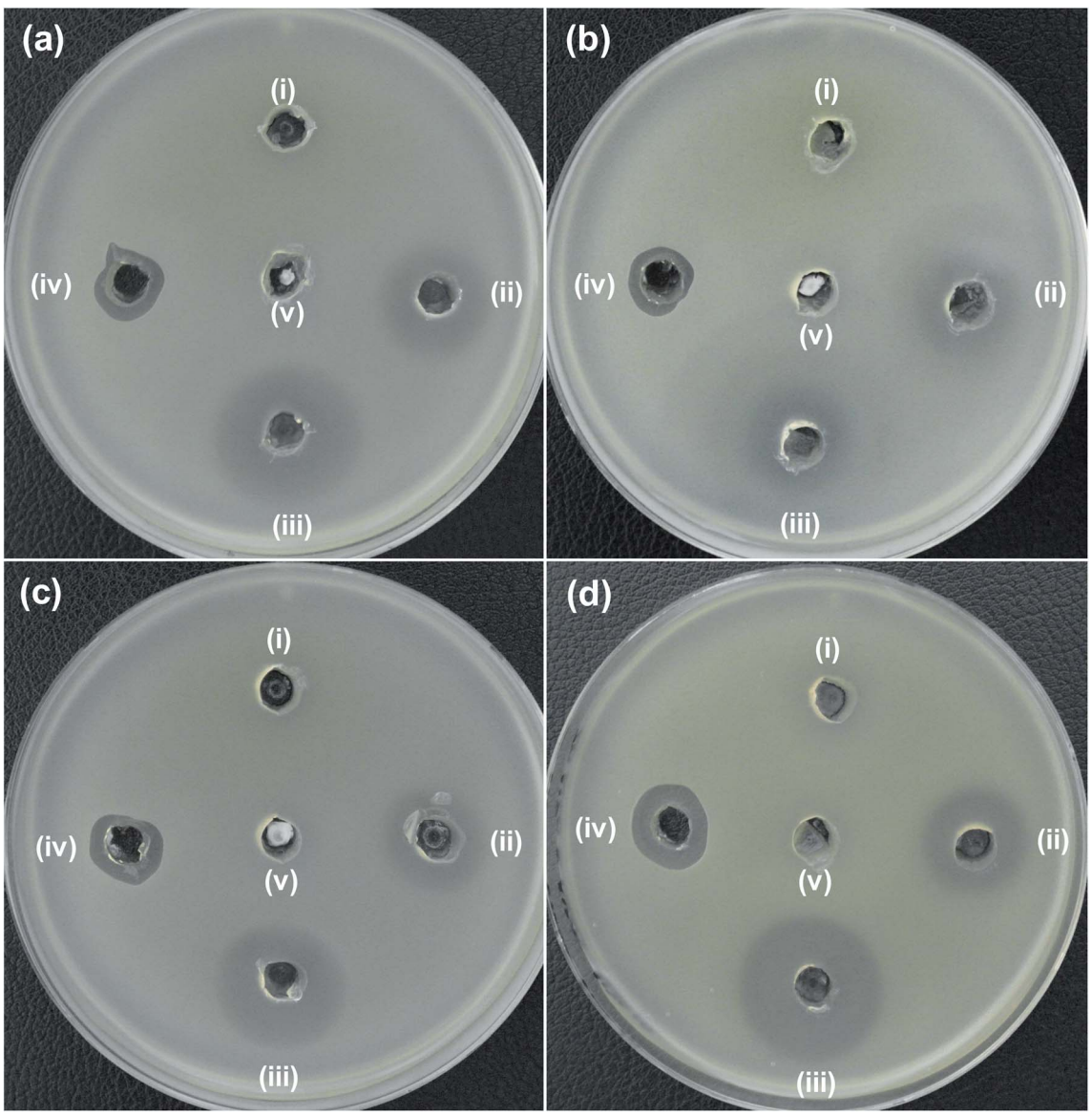

Fig. 6 Zone of inhibition (ZOI) of ZnO samples against MDR strains of *E. coli* (a) 1368, (b) BAA2452, and (c) 1A626 and an MDR strain of *A. baumannii* (d) 12001. Diameter of ZOI is also displayed in the Table 3 (average from $n = 3$).

Table 3 Zone of inhibition (ZOI) diameter of ZnO samples against drug resistant strains [(a) 1368, (b) BAA2452, (c) 1A626 of *E. coli* and ((d)12001] of *A. baumannii*. Data shown here is one of the representative from $n = 3$. N.D. indicates that the zone of inhibition was not detected

	Zone of inhibition (mm)				
Bacterial cells	(i) ZO	(ii) 2NZO	(iii) 5NZO	(iv) Polymyxin B	(v) DMSO
(a) *E. coli* 1368	N.D.	18	23	13	N.D.
(b) *E. coli* BAA2452	N.D.	14	17	12	N.D.
(c) *E. coli* 1A626	N.D.	18	21	12	N.D.
(d) *A. baumannii* 12001	N.D.	18	25	15	N.D.

grid used for TEM measurements. Elemental mapping of 5NZO (Fig. 2d–f) also indicates the presence of Zn, O, and Ni.

3.1.3 XPS spectra. XPS spectra display the binding energy signals of Zn 2p and Ni 2p from 5NZO (Fig. 3). XPS was performed to understand the oxidation state of chemical elements present in the 5NZO sample. Fig. 3a depicts the binding energy signals of Zn 2p, with strong signals observed at 1021.3 and 1044.4 eV, which can be assigned to the binding energies of Zn $2p_{3/2}$ and Zn $2p_{1/2}$, respectively.[35] The energy difference between Zn $2p_{3/2}$ and Zn $2p_{1/2}$ binding energy levels can be calculated as ~23.1 eV, which also confirms the existence of zinc as Zn^{2+} in the nanomaterial. Additionally, the doping of Ni^{2+} in the ZnO lattice was also confirmed by XPS (Fig. 3b). Fig. 3b shows the Ni 2p spectrum of the 5NZO sample, which was fitted into four peaks at 855.4, 861.5, 872.8, and 879.8 eV. The calculated value (17.4 eV) from the energy gap between the Ni $2p_{3/2}$ (855.4 eV) and Ni $2p_{1/2}$ (872.8 eV) peaks is very different from that of NiO (18.4 eV), confirming that nickel in the sample is not present in the form of NiO in ZnO lattice sites.[36] Moreover, the satellite peaks of Ni $2p_{3/2}$ (861.5 eV) and Ni $2p_{1/2}$ (879.8 eV) indicate the existence of Ni^{2+}, confirming successful doping of Ni^{2+} ion in the ZnO lattice.[37]

3.2 Antibacterial activity

3.2.1 Zone of inhibition (ZOI) and minimum inhibitory concentration (MIC). Agar well diffusion studies were performed to evaluate the antibacterial activity of Ni^{2+}-doped ZnO NPs. The zone of inhibition (ZOI) was examined in agar plates

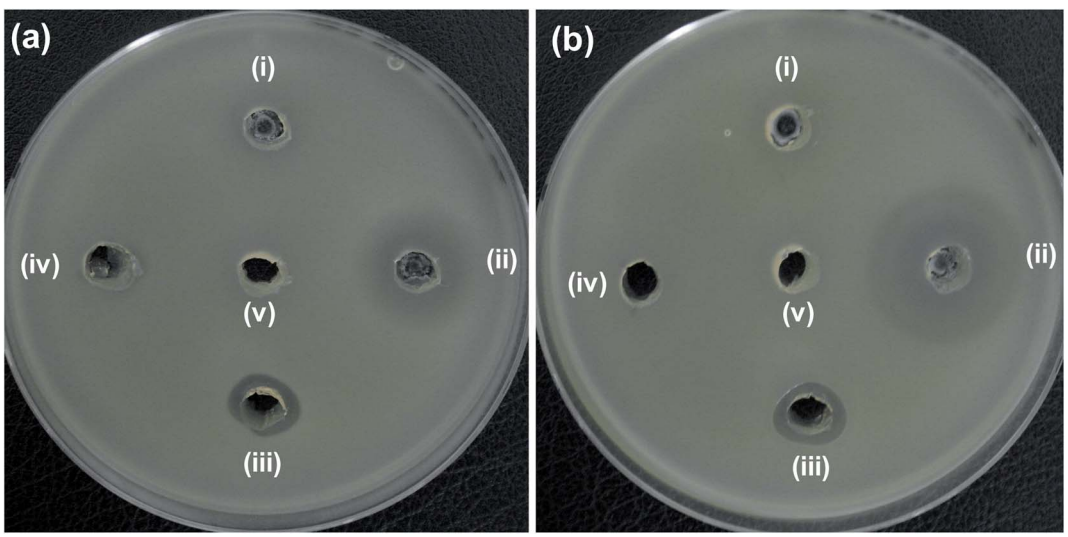

Fig. 7 Zone of inhibition (ZOI) of ZnO samples against *mcr-1* strains of *E. coli* (a) NCCP 16283 and (b) NCCP 16284. Diameter of ZOI is also displayed in the Table 4 (average from $n = 3$).

Table 4 Zone of inhibition (ZOI) diameter of ZnO samples against *mcr-1* strains [(a) NCCP 16283, (b) NCCP 16284] of *E. coli*. Data shown here is one of the representative from $n = 3$. N.D. indicates that the zone of inhibition was not detected

	Zone of inhibition (mm)				
Bacterial cells	(i) ZO	(ii) 5NZO	(iii) Polymyxin B	(iv) Erythromycin	(v) DMSO
(a) NCCP 16283	N.D.	22	13	N.D.	N.D.
(b) NCCP 16284	N.D.	24	13	N.D.	N.D.

Table 5 Minimum inhibitory concentration (MIC) of ZnO samples against (a) *E. coli*, (b) *A. baumannii*, MDR strains [(c) 1368, (d) BAA2452, (e) 1A626] of *E. coli* and [(f)12001] of *A. baumannii*. Data shown here is one of the representative from $n = 3$

		Minimum inhibitory concentration ($\mu g\ mL^{-1}$)	
Bacterial cells		ZO	5NZO
(a) *E. coli* ATCC25922		>250	200
(b) *A. baumannii* ATCC19606		>250	200
MDR strains	(c) *E. coli* 1368	>250	200
	(d) *E. coli* BAA2452	>250	200
	(e) *E. coli* 1A626	>250	200
	(f) *A. baumannii* 12001	>250	125

loaded with synthesized NPs (20 μL of 5 mg mL^{-1}) after 24 h of incubation at 37 °C. Fig. 4 shows the bacterial growth inhibition capacity of ZO, 2NZO, and 5NZO against Gram-negative bacterial strains, *E. coli* (Fig. 4a) and *A. baumannii* (Fig. 4b). The effective ZOI against *E. coli* for 2NZO and 5NZO samples were 18 and 24 mm, respectively (Table 1), and can act as polymyxin B (14 mm), a last-resort peptide antibiotic against Gram-negative bacteria, at the same concentration. The ZOI of 5NZO sample appears to be larger than the works reported.[32,38] Moreover, the ZOI was 12 mm for the 5NZO sample against *A. baumannii* (Table 1).

Additionally, the effectiveness of NZO NPs was evaluated for antibacterial activity toward the Gram-positive bacteria, *S. aureus* (Fig. 4c) and *S. epidermidis* (Fig. 4d). Although NZO NPs are active against Gram-positive bacteria (ZOI is 14 mm for 5NZO against both *S. aureus* and *S. epidermidis*) the activity of such NPs is much less than ampicillin and that for Gram-negative bacteria (ZOI is 24 mm for 5NZO against *E. coli*) (Table 1). This indicates that Gram-negative bacteria is better target for 2NZO and 5NZO. Therefore, further experiments focused on the MDR strains of the Gram-negative bacteria, *E. coli* and *A. baumannii* were performed.

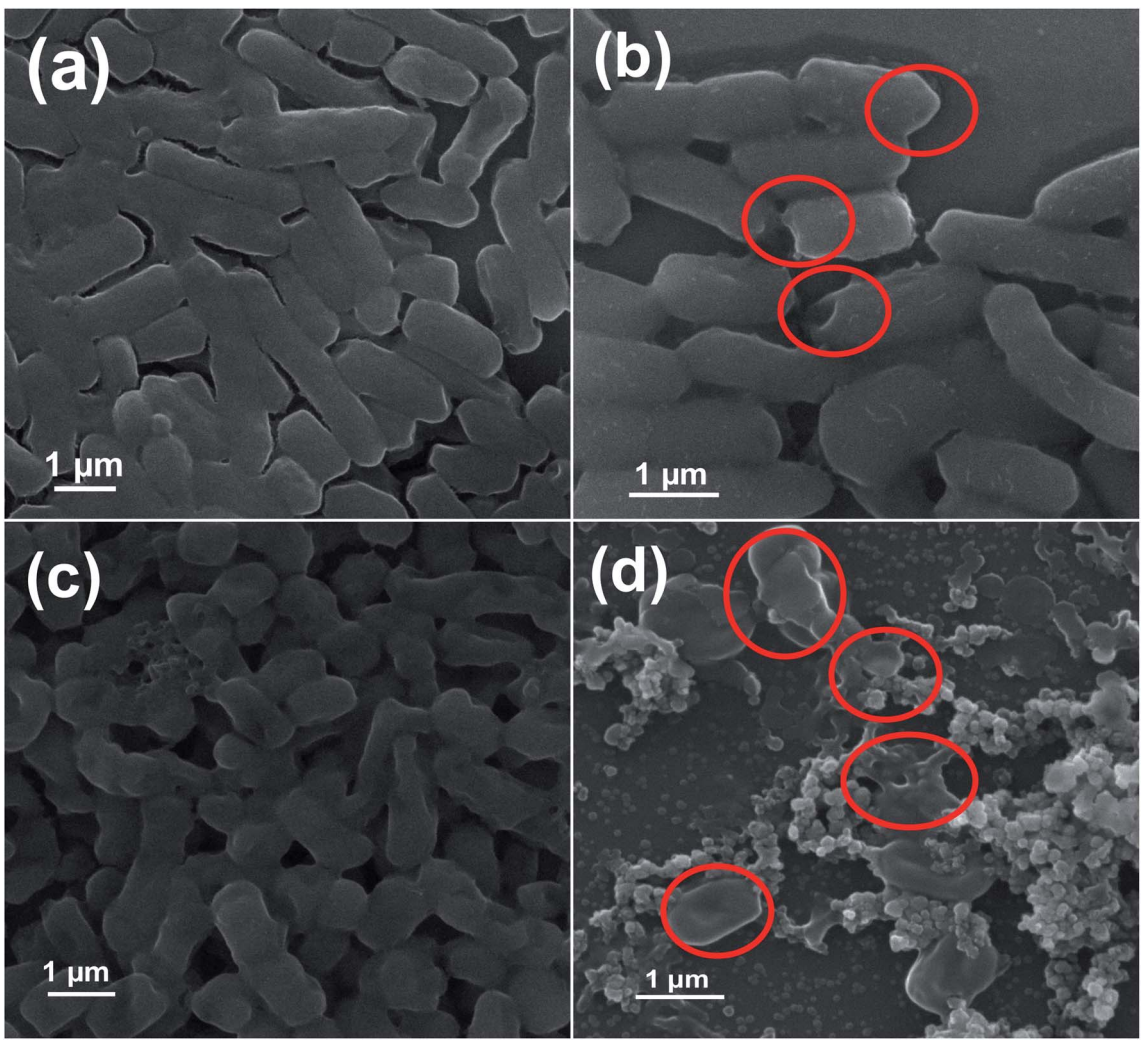

Fig. 8 Scanning electron microscopy (SEM) images of bacterial cells. Samples of *E. coli* (a) untreated and (b) treated with 5NZO. Samples of *A. baumannii* (c) untreated and (d) treated with 5NZO. Red circles indicate areas of cell membrane disruption.

Dependency on the concentration of the synthesized samples was also taken into consideration regarding antibacterial activity. Fig. 5 shows the ZOI of (a) ZO, (b) 2NZO and (c) 5NZO against *E. coli* at different concentrations. Diameter of ZOI is also displayed in the Table 2. As clearly seen form the Fig. 5 and Table 2 is that 5 mg mL^{-1} is the most active concentration of 5NZO samples to kill bacterial cells. Therefore, all samples were used with 5 mg mL^{-1} for future experiments.

The antibacterial activity of the synthesized NPs was investigated with regard to MDR strains of *E. coli* (Fig. 6a–c) and *A. baumannii* (Fig. 6d). As seen in Fig. 6, the 5NZO exhibit excellent antibacterial activity against MDR strains of *E. coli*, as the ZOI for 5NZO are 23, 17, and 21 mm against *E. coli* 1368, BAA2452, and 1A626, respectively (Table 3). Moreover, 5NZO showed a ZOI of 25 mm for an MDR strain of *A. baumannii* (12001), indicating that 5NZO is good activity toward Gram-negative bacteria and their MDR strains. Furthermore, 5NZO display comparatively better antibacterial activity than the other NPs (ZO and 2NZO) as the larger ZOI for 5NZO (Fig. 6). This high antibacterial activity of 5ZNO against Gram-negative bacteria and their MDR strains can be attributed to both an increase in Ni^{2+}-doping concentration along with a decrease in crystallite size.[24]

Additionally, clinical isolate of *E. coli* harboring *mcr-1* gene was also tested with 5NZO samples to evaluate its efficacy. ZOI (Fig. 7) and its corresponding diameter values (Table 4) showed that 5NZO sample can be an excellent antibacterial agent even against the clinical isolate of *E. coli* harboring *mcr-1* gene with 22 mm and 24 mm of ZOI for NCCP 16283 (Fig. 7a), NCCP 16284 (Fig. 7b) of *E. coli*, respectively.

We have also evaluated the MIC value of 5NZO sample for further approval of its antibacterial activity against Gram-negative bacterial cells and showed in Table 5. It can be clearly seen from the table that 5NZO sample not only act on wild type of bacteria[(a) *E. coli* (ATCC25922) and (b) *A. baumannii* (ATCC19606)] but also on their MDR strains [(c) *E. coli* 1368, (d) *E. coli* BAA2452, (e) *E. coli* 1A626, and (f) *A. baumannii* 12001]. Therefore, the synthesized 5NZO nanorods can be an effective nanoweapon against MDR strains of Gram-negative bacterial cells.

3.2.2 Morphological characterization of bacteria. Antibacterial effectiveness of NZO NPs was also investigated by SEM to evaluate the morphological changes of wild-type and MDR strains of *E. coli* and *A. baumannii* before and after exposure to the 5NZO. The SEM images of the bacterial cells are shown in Fig. 8 and 9. The untreated *E. coli* and *A. baumannii* cells (Fig. 8a and c, respectively) display a smooth and intact surface. However, some morphological changes, observed as membrane corrugations due to wrinkling and damage after treatment with 5NZO are observed, as indicated by red circled portions in Fig. 8b and d for treated *E. coli* and *A. baumannii*, respectively. Similar morphological changes are observed in Fig. 9, for the MDR strains of untreated *E. coli* (Fig. 9a, c and e) and *A. baumannii* (Fig. 9g), which exhibit smooth surfaces, whereas treatment of MDR strains of *E. coli* (Fig. 9b, d and f) and *A. baumannii* (Fig. 9h) with 5NZO exhibit wrinkled and damaged cell walls (indicated with red circles in Fig. 9b, d, f and h). The effectiveness of 5NZO for antibacterial activity can therefore be observed from the SEM micrographs. A plausible mechanism for antibacterial activity by 5NZO is the accumulation of 5NZO on the cell wall, resulting in increased cell permeability through cell membrane disruption.[23] It is likely that membrane disruption (supported by Fig. 8 and 9) in conjunction with generation of ROS are two feasible explanations for the antibacterial activity of 5NZO, as this allows for leakage of intracellular material, causing cell membrane shrinkage, and ultimately cell death.[23,24,26]

3.2.3 Production of reactive oxygen species (ROS) by NZOs. Among several known distinct mechanisms for ZO NPs as

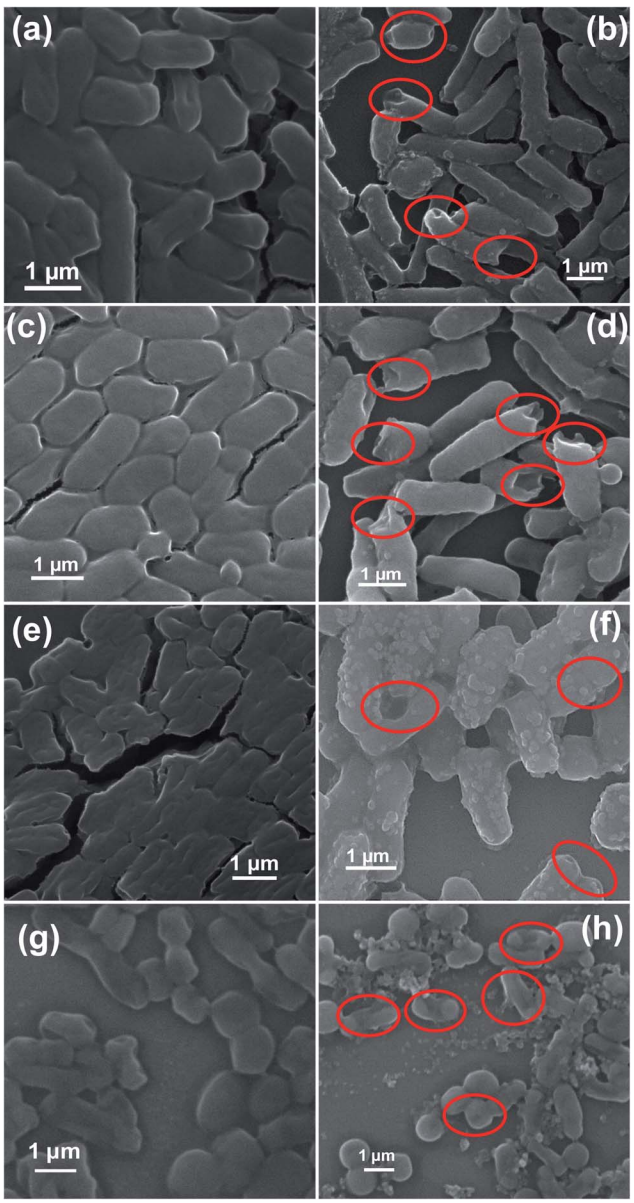

Fig. 9 Scanning electron microscopy (SEM) images of MDR strains of bacteria cells. Samples of *E. coli* 1368 (a) untreated and (b) treated; *E. coli* BAA2452 (c) untreated and (d) treated; *E. coli* 1A626 (e) untreated and (f) treated; *A. baumannii* 12001 (g) untreated and (h) treated. Treated cells were treated with 5NZO. Red circles indicate cell membrane disruption.

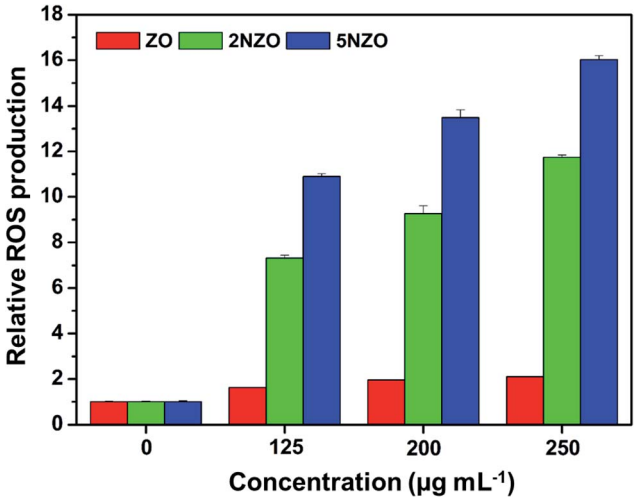

Fig. 10 Quantification of ROS production by using fluorescence dye. Fluorescence intensity at 520 nm of *E. coli* ATCC 25922 cells treated with ZO, 2NZO, and 5NZO, respectively, was measured. Bacteria cells treated with NPs in PBS are used as a blank for fluorescence detection. Three-independent experiments were performed. The data was processed using MARS Data Analysis software (ver. 3.02 R2; BMG Labtech) and relative ROS production by NPs were shown ($p < 0.05$).

antibacterial activity[23] the most effective antibacterial mechanism is the generation of reactive oxygen species (ROS), which directly leads to cell death by damaging functional cellular components such as DNA and proteins. Generally, NPs with larger specific surface areas and smaller crystallite sizes have been known to produce more ROS. It is also established that decreasing the crystallite size by Ni^{2+}-doping increased the surface area, resulting in improved antibacterial activity.[24] To prove that the NZOs synthesized in this study produce more ROS compared to ZO, we performed DCFH-DA assay to determine the cellular concentration of ROS by quantifying fluorescence emitted at 520 nm. We found that *E. coli* ATCC 25922 treated with NZOs generated approximately 7 to 16 times more ROS than that produced from ZO (Fig. 10). The 5NZO sample showed comparatively more ROS production than other samples. Therefore, our results corroborated with the previous results where 5NZO sample showed better antibacterial activity than other samples and the explanation can be attributed to the more ROS production.

4. Conclusions

In summary, this work demonstrates the low-temperature solution synthesis of Ni^{2+}-doped ZnO NPs and the resulting selective antibacterial activity against Gram-negative bacteria, *E. coli* and *A. baumannii* including their MDR strains and *mcr-1* associated colistin resistant *E. coli* strains. The 5% Ni^{2+}-doped ZnO (5NZO) NPs even showed comparatively better antibacterial activity at least by zone of inhibition method against Gram-negative bacteria compared to polymyxin B, a last resort peptide antibiotic that is currently used clinically as colistin. Moreover, NZOs produced more ROS compared to ZO. Because the method shown here is a cost-effective and includes simple synthetic strategy, these synthesized NPs can be used as a platform for the development of metal oxide nanomaterials for biomedical applications, in particular the design of nanoweapons against the ever-increasing public health threat of MDR bacteria.

Conflicts of interest

There are no conflicts to declare.

Acknowledgements

This work was supported by the National Research Foundation of Korea (NRF) grant funded by the Korean government (MSIT) [grant number 2018R1D1A1B07040941]. We are thankful to Prof. Hyun Deok Yoo at the Department of Chemistry, Pusan National University, for use of the X-ray diffractometer.

References

1 A. Naskar and K. S. Kim, *Microorganisms*, 2019, **7**, 356.
2 V. A. Kumar and S. Khan, *Indian J. Med. Res.*, 2015, **141**, 491–492.
3 J. O'Neill, 2016, available online, https://amr-review.org/sites/default/files/160525_Final%20paper_with%20cover.pdf, accessed on 2 October 2019.
4 W. A. McGuinness, N. Malachowa and F. R. DeLeo, *Yale J. Biol. Med.*, 2017, **90**, 269–281.
5 B. Li and T. J. Webster, *J. Orthop. Res.*, 2018, **36**, 22–32.
6 World Health Organization, *WHO publishes list of bacteria for which new antibiotics are urgently needed*, 2017, available online, https://www.who.int/news-room/detail/27-02-2017-who-publishes-list-ofbacteria-for-which-new-antibiotics-are-urgently-needed, accessed on 24 September 2019.
7 V. Tiwari, N. Mishra, K. Gadani, P. S. Solanki, N. A. Shah and M. Tiwari, *Front. Microbiol.*, 2018, **9**, 1218.
8 N. T. Mutters, A. Mampel, R. Kropidlowski, K. Biehler, F. Günther, I. Bălu, V. Malek and U. Frank, *Fitoterapia*, 2018, **129**, 237–240.
9 S. T. Odonkor and K. K. Addo, *Int. J. Microbiol.*, 2018, **2018**, 7204013.
10 G. C. Schito, K. G. Naber, H. Botto, J. Palou, T. Mazzei, L. Gualco and A. Marchese, *Int. J. Antimicrob. Agents*, 2009, **34**, 407–413.
11 H. Ellis and E. Schoenberger, *PLoS One*, 2017, **12**, e0170451.
12 A. DiGiandomenico and B. R. Sellman, *Curr. Opin. Microbiol.*, 2015, **27**, 78–85.
13 C. Torres-Barceló, *Emerg. Microb. Infect.*, 2018, **7**, 168.
14 J.-W. Xu, K. Yao and Z.-K. Xu, *Nanoscale*, 2019, **11**, 8680–8691.
15 A. Gupta, S. Mumtaz, C.-H. Li, I. Hussain and V. M. Rotello, *Chem. Soc. Rev.*, 2019, **48**, 415–427.
16 S. Tang and J. Zheng, *Adv. Healthc. Mater.*, 2018, **7**, 1701503.
17 X. Li, S. M. Robinson, A. Gupta, K. Saha, Z. Jiang, D. F. Moyano, A. Sahar, M. A. Riley and V. M. Rotello, *ACS Nano*, 2014, **8**, 10682–10686.

18 A. Naskar, S. Bera, R. Bhattacharya, P. Saha, S. S. Roy, T. Sen and S. Jana, *RSC Adv.*, 2016, **6**, 88751–88761.
19 J. Chen, S. Mao, Z. Xu and W. Ding, *RSC Adv.*, 2019, **9**, 3788–3799.
20 T. Verdier, M. Coutand, A. Bertron and C. Roques, *Coatings*, 2014, **4**, 670–686.
21 A. Naskar, H. Khan, R. Sarkar, S. Kumar, D. Halder and S. Jana, *Mater. Sci. Eng. C*, 2018, **91**, 743–753.
22 Z. Xiong, X. Zhang, S. Zhang, L. Lei, W. Ma, D. Li, W. Wang, Q. Zhao and B. Xing, *Ecotoxicol. Environ. Saf.*, 2018, **161**, 507–514.
23 A. Sirelkhatim, S. Mahmud, A. Seeni, N. H. M. Kaus, L. C. Ann, S. K. M. Bakhori, H. Hasan and D. Mohamad, *Nano-Micro Lett.*, 2015, **7**, 219–242.
24 K. R. Raghupathi, R. T. Koodali and A. C. Manna, *Langmuir*, 2011, **27**, 4020–4028.
25 S. B. Rana and R. P. P. Singh, *J. Mater. Sci.: Mater. Electron.*, 2016, **27**, 9346–9355.
26 R. S. Kumar, S. H. S. Dananjaya, M. D. Zoysa and M. Yang, *RSC Adv.*, 2016, **6**, 108468–108476.
27 H. B. Dias, M. I. B. Bernardi, V. S. Marangoni, A. C. de Abreu Bernardi, A. N. de Souza Rastelli and A. C. Hernandes, *Mater. Sci. Eng. C*, 2019, **96**, 391–401.
28 C. Karunakaran, V. Rajeswari and P. Gomathisankar, *Mater. Sci. Semicond. Process.*, 2011, **14**, 133–138.
29 G. Iqbal, S. Faisal, S. Khan, D. F. Shams and A. Nadhman, *J. Photochem. Photobiol., B*, 2019, **192**, 141–146.
30 A. Naskar, H. Khan and S. Jana, *Advanced Nano-Bio-Materals and Devices*, 2017, **1**, 182–190.
31 K. Vijayalakshmi and D. Sivaraj, *RSC Adv.*, 2015, **5**, 68461–68469.
32 A. H. Shah, M. B. Ahamed, D. Neena, F. Mohmed and A. Iqbal, *J. Alloys Compd.*, 2014, **606**, 164–170.
33 K. S. Ong, Y. L. Cheow and S. M. Lee, *J. Adv. Res.*, 2017, **8**, 393–398.
34 T. Zhou, M. Hu, J. He, R. Xie, C. An, C. Li and J. Luo, *CrystEngComm*, 2019, **21**, 5526–5532.
35 A. Naskar, S. Bera, R. Bhattacharya, S. S. Roy and S. Jana, *J. Alloys Compd.*, 2018, **734**, 66–74.
36 G. Vijayaprasath, R. Murugan, S. Palanisamy, N. M. Prabhu, T. Mahalingam, Y. Hayakawa and G. Ravi, *Mater. Res. Bull.*, 2016, **76**, 48–61.
37 R. S. Ganesh, E. Durgadevi, M. Navaneethan, V. L. Patil, S. Ponnusamy, C. Muthamizhchelvan, S. Kawasaki, P. S. Patil and Y. Hayakawa, *Chem. Phys. Lett.*, 2017, **689**, 92–99.
38 Z. Y. Dong, M. P. N. Rao, M. Xiao, H. F. Wang, W. N. Hozzein, W. Chen and W. J. Li, *Front. Microbiol.*, 2017, **8**, 1090.

